Solid Freeform Fabrication 2016: Proceedings of the 27th Annual International
Solid Freeform Fabrication Symposium – An Additive Manufacturing Conference
Reviewed Paper

LASER ADDITIVE MANUFACTURING PROCESSING OF A MIXTURE OF IRON AND NICKEL POWDERS

Joseph Tunick Strauss[*], Michael J. Stucky[†]

[*] HJE Company, Inc. 820 Quaker Rd., Queensbury, NY 12804
[†] Norwood Medical 2002 Webster St, Dayton, OH 45404

Key Words
Powder, Powder Mixture, Additive Manufacturing

Abstract

Laser-based powder bed additive manufacturing (AM) of metal powders uses pre-alloyed powder, which limits the alloys available for processing. Other processes using metal powders such as powder metallurgy (PM) (press and sinter and MIM (Metal Injection Molding)) and welding use elemental powder mixtures to produce a wide variety of alloy compositions. This study tests the ability of laser AM to produce a homogeneous alloy from a mixture of powders.

Introduction

The metal powders used in AM processes have strict specifications on particle size, particle size distribution, and morphology, which in turn affect the packing factor and flowability of the powder, two important attributes for AM. In addition, powder compositional homogeneity is important and this is fulfilled by the use of pre-alloyed powder. However, not all compositions of interest are available in powder form.

Several commercial processes involve the use of mixed metal powders where homogenization is achieved during the processing. Powder metallurgy (PM) processes commonly use mixes of elemental powder and master alloys. Press and sinter processing use atomized or reduced iron powder mixed with carbon and nickel to produce a wide variety of steels; the alloying is achieved during the sintering heat treatment via solid state diffusion (1). MIM can make a wide variety of stainless steels by mixing iron, nickel, and a master alloy. Again, homogenization takes place during the sintering heat treatment (2).

Many welding processes such as SMAW (Shielded Metal Arc Welding, commonly known as “stick welding”), FCAW (Flux Cored Arc Welding), and SMA (Submerged Arc Welding) use a carbon steel wire as the primary weld matrix material. Alloying elements in the form of powders are added to the flux and the alloying and homogenization occur in the melt pool during the time the material is molten (3).

In view of these other processes this current study is primarily the investigation of the degree of homogenization that can be achieved in the time scale of a laser weld in a powder bed laser additive manufacturing process.

The iron-nickel system was chosen for this investigation for the following reasons:

1. Iron and nickel are metallurgically compatible and are the basis for numerous commercially important alloys.
2. The laser absorbance of both iron and nickel are similar. This should avoid incongruent melting during the interaction of the laser.
3. The densities are similar. This should minimize gravity segregation during the powder transfer and manipulation of the AM equipment.
4. There is sufficient atomic number contrast (Z contrast) to enable clear identification of the individual elements in EDS (Energy Dispersive Spectroscopy).
5. Iron and nickel powder were readily available with equivalent particle size and particle size distributions.

Although the primary goal of this study is to determine the extent of homogeneity attainable using a mixture of metal powders, it is not the goal to make a specific alloy. However, emulating a known alloy allows us to extend the study to include physical properties as well. In light of this an alloy of 64Fe36Ni was chosen, also known as Invar 36 ®.

Methodology

The methodology used in this study entailed the following:

1. Obtain atomized iron and nickel powders and mix to a specific composition.
2. Print the parts via laser sintering at various operating parameters.
3. Metallographically prepare samples from the printed parts and examine.
4. Perform various physical property tests.

Powder: The iron and nickel powders were obtained from a commercial powder producer (4). The powders were produced by inert gas atomization, which yields a relatively spherical morphology. The powder was supplied as “MIM” grade, which refers to the particle size and particle size distribution being tailored for MIM applications. Table 1 summarizes the particle size and distribution of the powders. Table 1 also includes the particle size data for the mixture of powders.

Table 1. Summary of Particle Size and Distribution of Iron and Nickel Powders.

Powder	**Dmean**	**Std. Dev.**	**D95**	**D90**	**D50**	**D10**	**D5**
Fe	12.8	6.9	26.8	22.2	11.7	4.6	3.6
Ni	12.5	6.2	24.5	20.7	11.7	4.9	3.9
64Fe 36Ni mix	12.6	6.9	25.4	21.3	11.7	4.8	3.8

(Analysis via Microtrac S3500. All data in microns.)

The data in Table 1 show that the particle size and distribution of the Fe and Ni powders were equivalent and the mixture of the two powders was essentially indistinguishable from either parent powder. Table 2 summarizes bulk powder properties: flow rate, apparent and tap densities, and the Hausner ratio. None of the powders were free-flowing, which is predicted by the Hausner ratio. The apparent and tap densities were relatively high with respect to typical

"additive manufacturing" grade powders for powder bed laser sintering applications. However, these bulk properties are representative of MIM grade powder.

Table 2. Summary of Bulk Powder Properties.

Powder	**Flow, sec/50 grams**	**$\rho_{apparent}$, % theoretical**	**ρ_{tap}, % theoretical**	**$\rho_{theoretical}$**	**Hausner ratio**
Fe	No Flow	3.2, 41%	4.4, 56%	7.87	1.38
Ni	No Flow	3.6, 40%	5.0, 56%	8.91	1.39
64Fe 36Ni mix	No Flow	3.3, 40%	4.6, 56%	8.24	1.39

All density data are in g/cm^3. Flow, $\rho_{apparent}$, ρ_{tap}, measured as per MPIF 28, MPIF 48, and MPIF 46. The $\rho_{theoretical}$ of the powder mixture was calculated from rule of mixtures.

Table 3 summarizes the chemical analyses of the iron and nickel powders. Also included in this table is the chemistry of the 64Fe36Ni powder mixture as determined by the rule of mixtures and the ASTM chemical specification for Invar 36 ®. It should be noted that the mixture of powders does not produce a 64Fe36Ni but rather an alloy with 62.6% iron due to the other elements within the chemistry of the initial powders.

Table 3. Summary of the Chemical Analyses of the Iron and Nickel Powders.

Powder	**Fe**	**Ni**	**Mn**	**Cr**	**Si**	**C**	**S**	**P**
Fe powder	Bal	0.31	0.93	0.57	0.42	<0.01	-	0.007
Ni powder	0.15	Bal	0.013	-	0.016	0.01	-	-
64Fe 36Ni mix	62.6	36.1	0.60**	0.36**	0.27	<0.01	-	0.004
Invar 36® *	Bal	36.0	0.50	0.25	0.40	.05	0.015	0.015

* ASTM F1684-06 specification with maximum limits of impurities.
** Outside of ASTM F1684-06 specification.

Laser Sintering Equipment and Operating Parameters: The equipment used to print the samples was a Phenix PXM (3D Systems) unit with a laser rating of 300 watts. Table 4 summarizes the equipment and the operating parameters. The Phenix PXM machine was chosen as it has the capability to process "unflowable" powders such as the ones chosen for this study. All of the build parameters were held constant with the exception of the laser power. Samples, cubes nominally 20 mm per side, were built with 75% (225 watts) and 100% power (300 watts). Figure 1 shows the as-built sample cubes. The figure shows different surface artifacts depending on the orientation. The left cube shows the as-printed top of the build. The center cube shows the bottom surface left by the wire EDM after removal from the build plate. The right cube shows a side of a cube. The top surface is shiny whereas the side appears brown from the iron oxide on the surface. This oxidation is not an indication on poor alloying with areas of unalloyed iron, which subsequently oxidizes. Rather, it is powder from the powder bed that has lightly sintered to the surface of the cube as it is built. This unsintered powder is primarily iron and it oxidized after the build was completed. This oxidized material is not part of the build and is easily removed by bead blasting. The top surface is shiny as it is the last surface processed and it was not exposed to fresh powder after the build was completed.

Table 4. Summary of Equipment and Operating Parameters.

Attribute	
System	Phenix PXM (3D Systems)
Maximum laser power	300 watts
Laser wavelength	1070 nm
Powder layer thickness	30 microns (pre-scan)
Scan	+/- 45 degrees, zero overlap
Beam speed	2500 mm/sec.

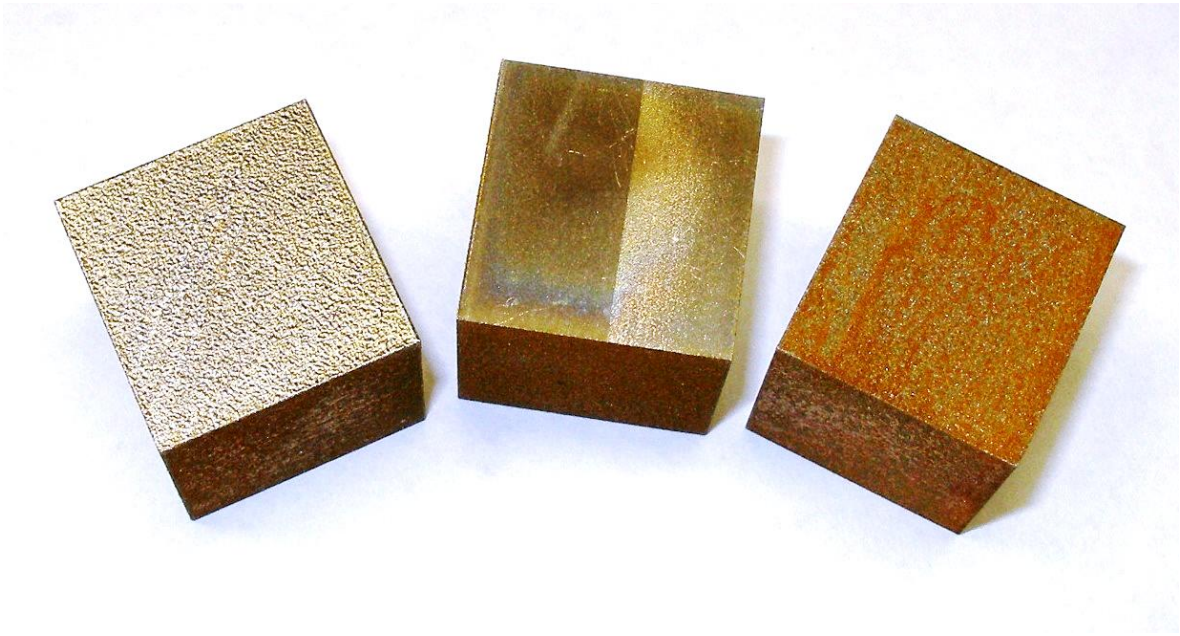

Figure 1. As-printed samples, nominally 20 mm per side. Left: top surface. Middle: bottom surface (after EDM removal from build plate). Right: side surface.

Metallographic Examination: The samples were prepared using standard metallographic techniques. The orientations viewed were from the top and side. Images were made by scanning electron microscope (SEM) backscatter electron imaging (BEI) on unetched surfaces at an accelerating voltage of 20 keV. Magnifications of 500x and 1000x were used. Differences in atomic number of the elements produce a contrast using BEI, with lower atomic numbers appearing darker. Thus in these images the iron appears dark and the nickel appears comparatively light. Alloyed areas appear as intermediate levels of gray. In addition, energy dispersive x-ray spectroscopy (EDS, Kα emission) was used to further identify the individual elements. The EDS dot scan information was color coded, red for iron and blue for nickel, and these scans overlaid on the BEI images. Figure 2 shows the grayscale BEI image with the EDS overlay in colors for the print made at 75% power, as-printed, in the side orientation view. Figure 3 shows the top view of the same sample. It is clear from the gray and color contrast that the microstructure is not compositionally homogenous. The size of the areas of greatest contrast agrees with the size of the largest particles of the initial powder. This implies that there was not sufficient power or energy density to fully melt and homogenize the material. Figure 4 is a BEI gray scale image with a line scan showing the variations in composition across a random line in the microstructure. The line scan plots 50 points. Although there is significant variation from

point to point, the overall composition is in agreement with the target composition of 64 iron and 36 nickel. It should be noted that this is a qualitative analysis as the other impurities were not accounted for and the nickel was determined by the remaining balance.

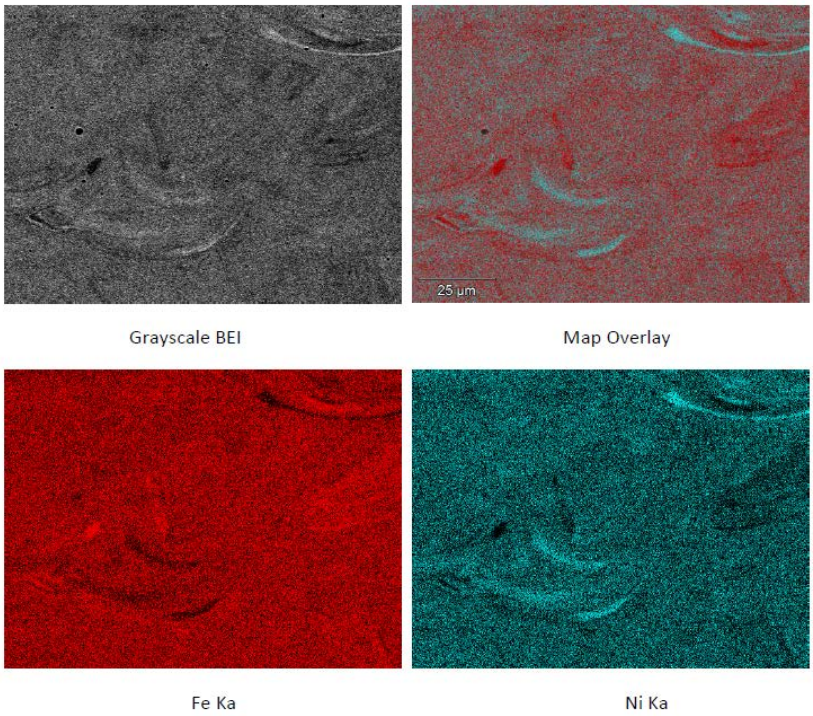

Figure 2. Microstructure of a part printed at 75% power, side orientation.

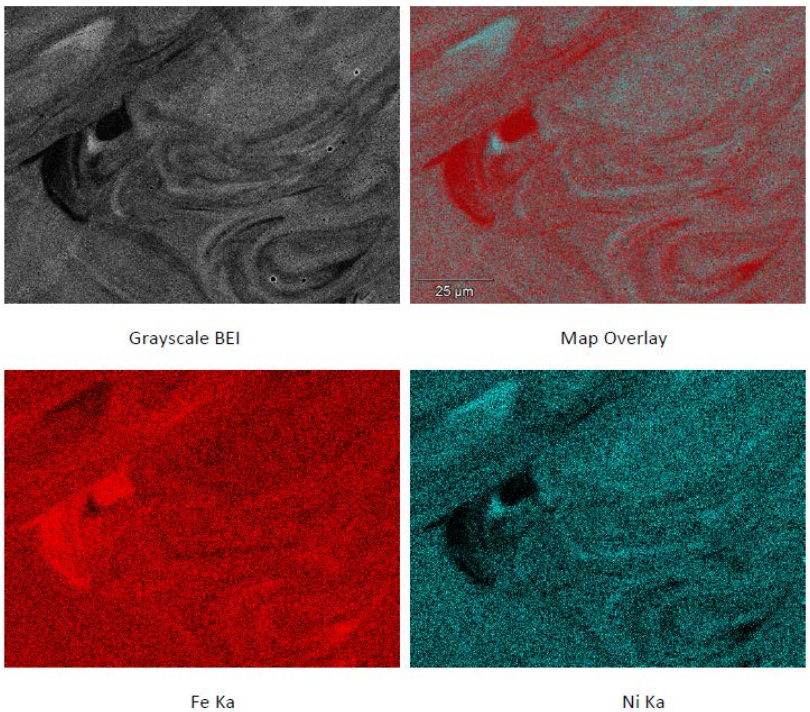

Figure 3. Microstructure of a part printed at 75% power, top orientation.

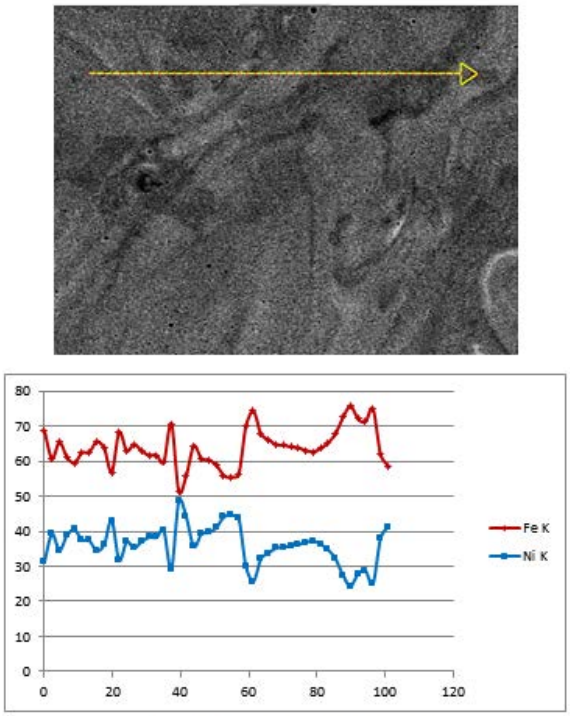

Figure 4. BEI gray scale image of a part printed at 75% power (top view) with line scan showing compositional variations across a random line in the microstructure.

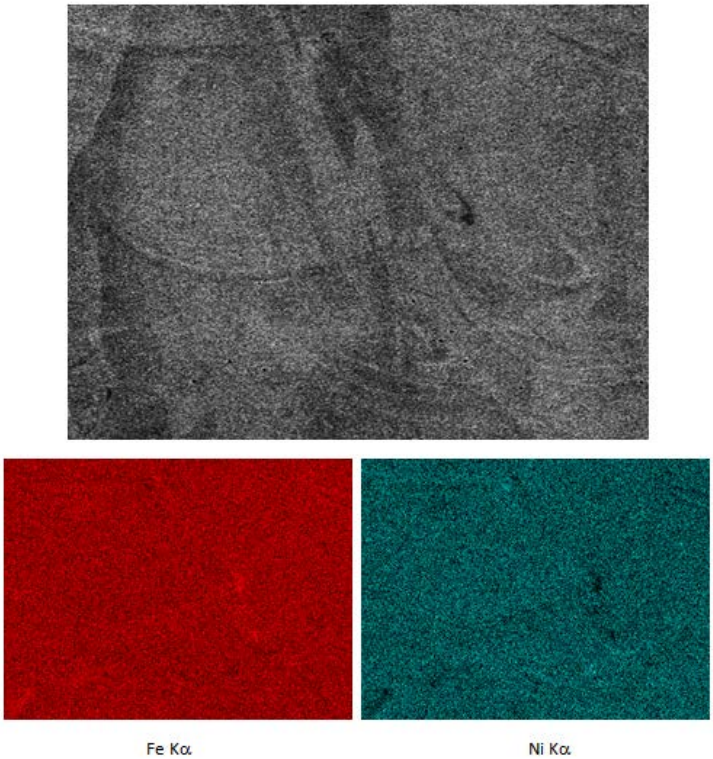

Figure 5. Gray scale image and colored EDS elemental map of a print made at 100% power. The image is from the side.

Figure 5 shows the gray scale image and colored EDS elemental maps of the side cross section of a print made at 100% power. The degree of homogeneity is much improved over that of the print made at 75% power. Figure 6 shows a gray scale BEI image of a print made at 100% power with a line scan showing the composition at various points along a line. The compositional scan is more uniform than that of prints made at 75% power (see Figure 4).

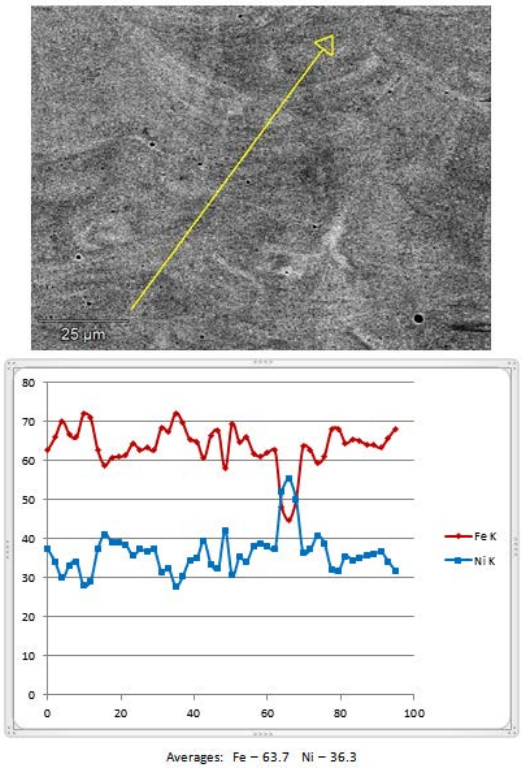

Figure 6. BEI gray scale image of a part printed at 100% power (side view) with line scan showing compositional variations across a random line in the microstructure.

In order to improve the compositional homogeneity of the as-printed part, a part printed at 75% power was heat treated at 1310 C for 90 minutes in a hydrogen atmosphere. This heat treatment is similar to the sintering cycle for an iron-nickel MIM part made from elemental powders (5). Figure 7 shows the BEI gray scale image and the colored EDS elemental maps of the top cross section of a part printed at 75% power after the heat treatment. The degree of homogeneity is very uniform. Figure 8 is the BEI gray scale image of the heat treated part and the line scan of the composition. The small amount of variation in composition along the random line also indicates that this sample has a high degree of compositional homogeneity. Thus, a post-print heat treatment can be used to improve the homogeneity of the as-printed part.

Physical Property Testing: The printed parts were subjected to mechanical and thermomechanical testing for comparison to conventionally produced (wrought) material. Mechanical testing consisted of hardness and density measurements. The hardness testing is summarized in Table 5. The materials labeled as Invar 36® ref refer to specifications for a commercially produced material (6). The materials labeled as Invar 36® are from commercially produced Invar 36® cold drawn to ½" rod.

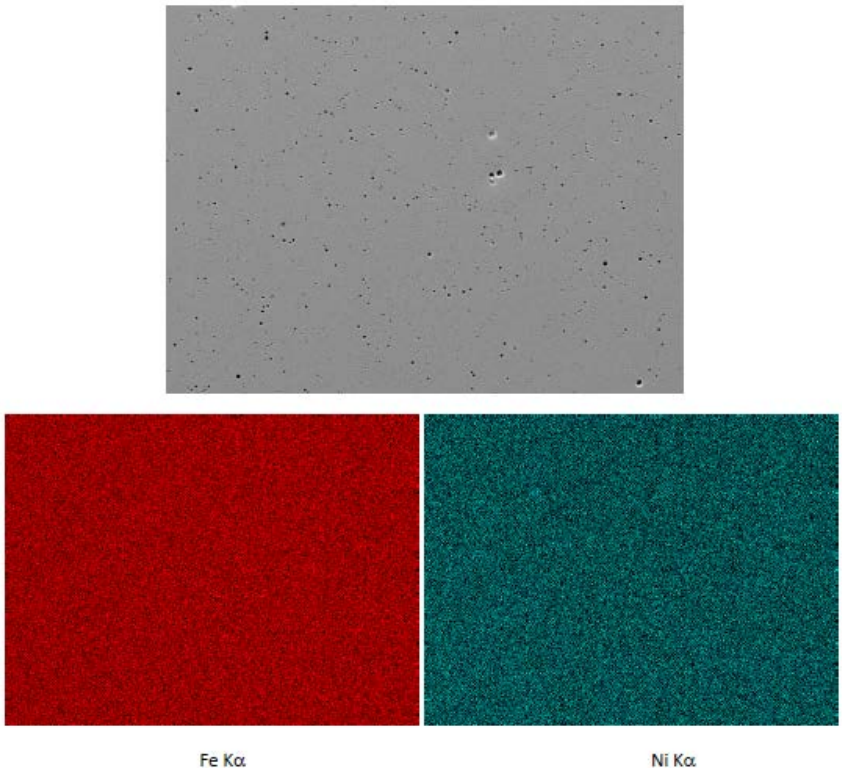

Figure 7. Gray scale image and colored EDS elemental map of a print made at 75% power and heat treated. The image is from the top.

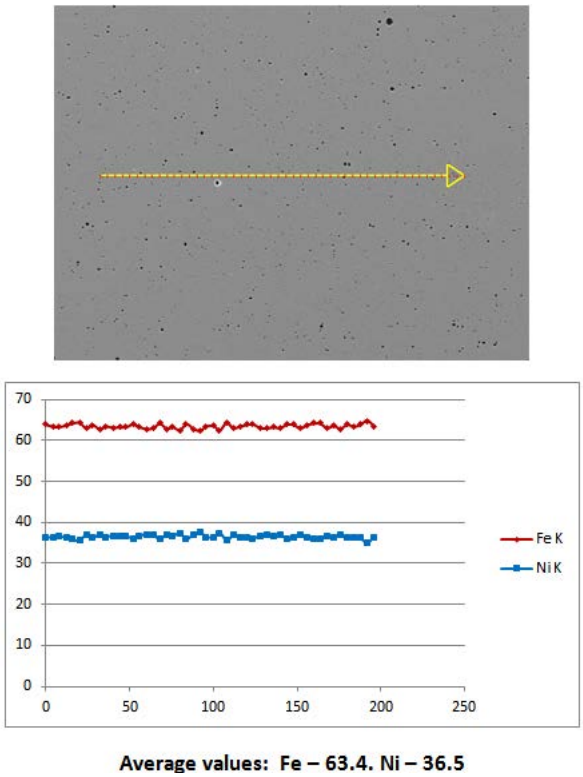

Figure 8. BEI gray scale image of a part printed at 75% power after the heat treatment (top view).

Table 5. Summary of Hardness Testing (average of 10 measurements).

Material	**Form**	**HRB**
Invar 36® ref	Cold drawn	90-98
Invar 36® ref	Annealed @ 815 C	70
Invar 36®	Cold drawn	97.2
Invar 36®	Annealed@ 815 C	65.1
Invar 36®	HT @ 1310 C	60.1
75% power	As-printed	82.4
75% power	Annealed@ 815 C	82.6
75% power	HT @ 1310 C	72.5
100% power	As-printed	82.4
100% power	Annealed@ 815 C	82.2
100% power	HT @ 1310 C	68.7

The hardness data on the Invar 36 is in good agreement with the reference data. The heat treated hardness is lower than the annealed hardness, which is to be expected as the heat treatment was performed at a higher temperature than the anneal. The hardness of the printed parts did not achieve the hardness of the cold drawn commercial material. This is expected as the microstructures of the as-printed parts are essentially that of a weldment (casting) rather than a cold worked microstructure. The as-printed hardness and the printed material after an 815 C anneal had equivalent hardnesses. This implies that the laser processing produces material in the annealed form. Heat treatment of the printed parts at 1310 C reduced the hardness significantly. The higher hardnesses of the printed parts compared to the annealed of heat treated wrought material was not explored further but is most likely from a grain size effect.

Table 6. Summary of Density Tests (as per MPIF 54, ASTM B 311).

Material	**Form**	**Density, g/cm^3**
Invar 36 ®ref	Cold drawn	8.05-8.20
Invar 36®	Cold drawn	8.16
Invar 36®	Annealed@ 815 C	8.16
Invar 36®	HT @ 1310 C	8.15
75% power	As-printed	8.14
75% power	Annealed@ 815 C	8.14
75% power	HT @ 1310 C	8.14
100% power	As-printed	8.14
100% power	Annealed@ 815 C	8.14
100% power	HT @ 1310 C	8.15

The density of each sample was determined using MPIF 54/ASTM B 311 (Archimedes method). All of the samples including the commercial wrought material were essentially identical and within the specification for commercially produced material.

The coefficient of thermal expansion (CTE) of this composition is a function of many process variables (7) including composition (primarily % Ni), impurities (most affected by C, Cr, and Mn), microstructure, % cold working, and thermal history (anneals, etc.). Figure 9 is a plot showing the variation to be expected in commercially produced 64Fe36Ni. It can be seen that at lower temperatures the amount of variation can be +/- 75% from the mean and at higher temperatures can be +/- 10%.

The CTE was measured using a dilatometer. Since the CTE of the 64Fe36Ni alloy varies with temperature the CTE was reported at two temperatures (260 C and 371 C). The data reported in Table 7 is the average of the CTE measured on the heat up and the cool down. All of the data of the printed samples are from samples oriented in the Z direction unless otherwise noted.

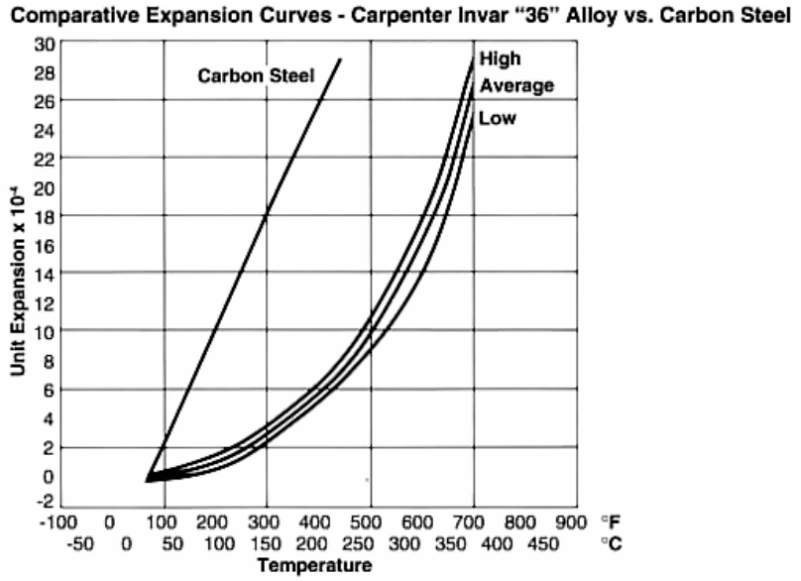

Figure 9. A plot of variation in CTE vs. Temperature for Invar 36® (6).

In general, the CTE's of the printed samples fell within the range suggested by the plot in Figure 9. The CTE data for the commercially produced Invar 36 showed a small variance overall. The variation in the CTE's of the printed parts showed more variation. This may be related to the difference in microstructure (printed "cast" vs. wrought) and remaining compositional variations.

Table 7. Summary of Coefficient of Thermal Expansion (CTE) Data.

Material	**Form**	**CTE at 260 C, ppm cm/cm/C**	**CTE at 371 C, ppm cm/cm/C**
Invar 36® ref	Cold drawn	3.4-5.0	7.3-8.4
Invar 36®	Cold drawn	4.1	7.2
Invar 36®	Annealed@ 815 C	4.0	7.3
Invar 36®	HT @ 1310 C	3.9	7.3
75% power	As-printed	4.5	7.5
75% power	Annealed@ 815 C	4.3	8.0
75% power	HT @ 1310 C	5.1	7.5
75% power	As printed, transverse	4.7	8.1
100% power	As-printed	4.6	7.1
100% power	Annealed@ 815 C	4.1	6.8
100% power	HT @ 1310 C	4.9	7.3
100% power	As printed, transverse	4.7	7.5

Conclusions

1) A mixture of iron and nickel powders was successfully printed by laser sintering.
2) The microstructural/compositional homogeneity of the as-printed parts was improved by increasing the laser power.
3) The microstructural/compositional homogeneity can be improved by the addition of a post-print heat treatment.
4) The mechanical properties (density, hardness) of the printed parts were comparable with the commercially produced Invar 36® alloy.
5) The thermomechanical properties (CTE) of the printed parts were generally within the range expected from this alloy. The data scatter of the printed parts was greater than that of the commercially produced Invar 36® alloy.

Acknowledgements

The authors would like to thank Tom Murphy and the Hoeganaes Corporation for generously providing the critical metallographic and analytical services.

References

1. F. V. Lenel, *Powder Metallurgy Principles and Applications* (Princeton, NJ: MPIF, 1980), 270-271.
2. Animesh Bose, Advances in Particulate Materials (Newton, MA: Butterworth-Heinemann, 1995), 305.

3. Charlotte Wiesman, ed., Welding Handbook, vol.1 (Miami, FL: AWS, 1976), 7, 9.
4. Sandvik Osprey Limited, Neath, UK.
5. Matthew Bulger, private communication with author, NetShape Technologies, 19 April, 2016.
6. Carpenter Technology Corporation, Technical Data Sheet: Carpenter Invar 36 ® Alloy, 3/15/04.
7) William S. McCain, Robert M. Maringer, “Mechanical and Physical Properties of Invar and Invar-Type Alloys”, (Report DMIC Memorandum 207, Battelle Memorial Institute, 1965).